Environmental Chemistry Letters (2020) 18:1413–1422
https://doi.org/10.1007/s10311-020-01008-7

ORIGINAL PAPER

# Higher dye degradation using a visible-light photocatalyst made of mesoporous graphitic carbon nitride prepared with the Tween-40 surfactant

**Barbara Ronara Machado de Lima[1,2] · Nilson Machado Pontes do Nascimento[1,2] · José Roberto Zamian[1,2] · Carlos Emmerson F. da Costa[1,2] · Luis Adriano Santos do Nascimento[1,2] · Sanclayton Geraldo Carneiro-Moreira[3] · Geraldo Narciso da Rocha Filho[1,2]**

Received: 5 December 2019 / Accepted: 10 April 2020 / Published online: 23 April 2020


## Abstract

Water pollution by organic pollutants such as textile dyes is a serious problem that could be solved by advanced photocatalytic semiconductors. Here we synthesized a visible-light photocatalyst made of mesoporous graphitic carbon nitride using the surfactant Tween-40, and we compared the surfactant performance in degrading rhodamine B with graphitic carbon nitride prepared by conventional methods. The toxicity of the photocatalyst was evaluated using bioassays with *Allium Cepa*. Results show that 93.0% of the rhodamine B was degraded by the new catalyst after 60 min under visible-light irradiation, whereas bulk graphitic carbon nitride and mesoporous graphitic carbon nitride with Pluronic F127 degraded only 30.5 and 86.0% of rhodamine B, respectively. We also found no ecotoxicity of the new catalyst. Higher degradation performance of the photocatalyst is explained by synergistic effect of nitrogen vacancies combined with the higher number of structural defects and more active sites, and by a better separation and transport of photogenerated charges of the synthesized mesopore catalyst, thus inducing a better response under visible light.

**Keywords** Tween-40 · Mesoporous · Graphitic carbon nitride

## Introduction

In the last decades, research on the development of systems is capable of remedying damage to the environment and studies that make it possible to generate clean energy have grown (Kumar et al. 2019). In this context, heterogeneous photocatalysis emerges, which enables the use of semiconductors in applications such as power generation clean, for example, in water cleavage for hydrogen production (Wang et al. 2016; Ruan et al. 2018; Wu et al. 2019) or in the photodegradation of organic pollutants, as in degradation of textile dyes (Osman et al. 2017; Zhang et al. 2019).

Graphitic carbon nitride (g-$C_3N_4$) has stood out among heterogeneous photocatalysis because it is stable in aqueous, acidic or basic solution, and its activation occurs in visible light (Chen et al. 2016). However, the photocatalytic efficiency of bulk graphitic carbon nitride is low due to its high electron–hole pair recombination rate, small pore volume, low surface area and, consequently, low active surface (Wang et al. 2016; Ruan et al. 2018). To improve this efficiency, several modifications have been made to the structure of the graphitic carbon nitride, for example, obtaining mesoporous graphitic carbon nitride (Tan et al. 2017), metal doping (Tonda et al. 2014; Gong et al. 2015) and heterojunctions (Li et al. 2014) among others.

The development of effective strategies for the production of mesoporous graphitic carbon nitride from soft template method (Liang et al. 2008) has been of interest to many

**Electronic supplementary material** The online version of this article (https://doi.org/10.1007/s10311-020-01008-7) contains supplementary material, which is available to authorized users.

✉ Geraldo Narciso da Rocha Filho
geraldonrf@hotmail.com

[1] Laboratory of Catalysis and Oilchemistry, Federal University of Pará, Guamá, Belém, PA 66075-110, Brazil

[2] Laboratory of Amazon Oils and Graduate Program of Chemistry, Federal University of Pará, Guamá, Belém, PA 66075-110, Brazil

[3] Physics Faculty, Federal University of Pará, Guamá, Belém, PA 66075-110, Brazil

researchers. Several works have been developed by using surfactants such as: Triton-X (Wang et al. 2010), Pluronic P123 (Yan 2012), Pluronic F127 (Wang et al. 2010), alginate (algal polysaccharide) and gelatin (polypeptide) (Zhang et al. 2013a) for photocatalysis applications for hydrogen production from water cleavage (Yan 2012), photoelectrochemistry (Wang et al. 2011) and rhodamine B degradation (Peer et al. 2017).

Applications of catalysts for water purification have some limitations, as radicals formed on the surface of the photocatalyst in sunlight can degrade pollutants, in addition to natural organisms. A sustainable photocatalyst should only degrade pollutants and be completely harmless to environmental flora (Ma et al. 2017).

Pluronic F127 and Tween-40 are low cost, biodegradable, nonionic surfactants (Poła and Ćirin 2012). In the literature, few works have been published by using these surfactants in the soft template method.

Polysorbates, such as Tween-40, are mainly used in the formulation of protein compounds (Kishore et al. 2011). However, they can also be used as synthetic molds for mesoporous materials. There are several studies using the polysorbate Tween-20, Tween-40, Tween-60 and Tween-80 (Boissière et al. 2000; García-Benjume et al. 2009; Chen et al. 2011; Xiong et al. 2012) as a guide for mesoporous structures. However, as far as is known, there are no reports on the synthesis of mesoporous graphitic carbon nitride by the soft template method with the Tween-40 surfactant.

Thus, this research proposes an innovative approach for the synthesis of graphitic mesoporous carbon nitride using Tween-40 as a surfactant, in addition to making a comparison with a surfactant reported in previous works, Pluronic F127, which still faces synthetic challenges. The effect of the use of surfactants on the synthesis of graphitic carbon nitride was evaluated through photocatalytic performance in the degradation of rhodamine B under irradiation of visible light. In addition, *Allium Cepa* bioassays were performed to demonstrate the macroscopic effects of Tween-40 synthesized catalyst and dye degradation products on the environment flora.

## Experimental

### Materials

Tween-40 (polyoxyethylenesorbitan monopalmitate, $C_{62}H_{123}O_{26}$), Pluronic F127 (polyoxyethylene-polyoxypropylene block copolymer, $EO_{100}PO_{65}EO_{100}$), melamine ($C_3H_6N_6$), benzoquinone ($C_6H_4O_2$), ammonium oxalate monohydrate ($(NH_4)_2C_2O_4{\cdot}H_2O$), isopropyl alcohol ($(CH_3)_2CHOH$), rhodamine B, sulfuric acid ($H_2SO_4$), ethyl alcohol ($CH_3CH_2OH$) and deionized water were all purchased from Sigma-Aldrich, Ltd. (Brazil). The reagents used for the photocatalysts synthesis are all of high-purity analytical grade and were not submitted to any purification treatment.

### Synthesis of photocatalyst

Mesoporous graphitic carbon nitride with Tween-40 and mesoporous graphitic carbon nitride with Pluronic F127 were successfully synthesized using the method proposed by Yan (2012) with modifications, described next. Initially, 1 g of melamine was added to 20 mL of deionized water. Then, 1.5 mL of sulfuric acid solution ($H_2SO_4$, 1:1 v/v) and 0.5 g of surfactant (Tween-40 or Pluronic F127) were added and then kept under reflux at 100 °C for 1 h, and the product was collected by filtration, washed with deionized water and ethanol and then dried at 80 °C for 12 h. The white powder obtained is the polymeric precursor of mesoporous graphitic carbon nitride, called of the polymeric precursor with Tween-40 and polymeric precursor with Pluronic F127. The polymeric precursors of graphitic carbon nitride with Tween-40 and the polymeric precursor with Pluronic F127 were calcined at 550 °C (2.5 °C/min, 240 min) under flow of nitrogen of 50 mL/min, and this yielded the mesoporous graphitic carbon nitride with Tween-40 and mesoporous graphitic carbon nitride with Pluronic F127. The bulk graphitic carbon nitride was synthesized of melamine polymerization at 550 °C (2.5 °C) for 2 h under nitrogen flow (50 mL/min).

### Characterization

Thermogravimetric and differential thermogravimetric (TG–DTG) analysis was carried out to obtain the thermogravimetric data (TG and DTG curves) under range of 24–1000 °C, at a heating rate of 10 °C/min under nitrogen gas flow (50 mL/min), with a thermal analyzer (Shimadzu, TGA-DTA, DTG-60H).

X-ray diffraction (XRD) was performed using a Bruker D8 Advance, with CuKα ($\lambda = 1.5406$ Å), and the scan rate employed was 0.2°/min for a $2\theta$ (5°–80°).

Photoluminescence spectra (PL) were measured using a USB Ocean Optics, and time-resolved photoluminescence spectroscopy signal was acquired through a Horiba, Delta Flex, equipped with light-emitting diode (LED), 352 nm (Supplementary Material, Figure S1).

Measurements of ultraviolet–visible diffuse reflectance spectra (DRS) were measured using spectrophotometer (ISR-2600, Shimadzu) using barium sulfate ($BaSO_4$) as reference (Supplementary Material, Figure S2).

The morphologies of the samples were examined using scanning electron microscopy (SEM, Tescan, Vega3 microscope) which was performed at an accelerating voltage of

20 kV and transmission electron microscopy (TEM, FEI Tecnai G2T20) (Supplementary Material, Figure S3).

Surface area, pore diameter and volume were calculated according to the Brunauer–Emmett–Teller and Barrett–Joyner–Halenda (BET/BJH) method using a Micromeritics Vacprep061-Degas System with treatment for degassing at 200 °C for 2 h (Supplementary Material, Table S1).

### Photocatalytic performance

Photocatalytic activity was evaluated by degradation of rhodamine B under visible-light irradiation using a 120-W metal vapor lamp at room temperature. More precisely, 50 mg of photocatalyst was added to 100 mL of rhodamine B (10 mg/L). Prior to irradiation it was stirred in the dark for 30 min. At 15-min intervals of irradiation exposure for 120 min, the photocatalytic mechanism of rhodamine B degradation was performed, Yan et al. (2009) and Fang et al. (2015), with the addition of hydroxyl ($^{\cdot}OH$), superoxide ($^{\cdot}O_2^-$) and hole ($h^+$) radical markers, such as isopropyl alcohol (1%), benzoquinone (10 mM) and ammonium oxalate (10 mM). During the photocatalytic test, at regular intervals, 3 mL of the suspension was collected, centrifuged and analyzed using a spectrophotometer ultraviolet–visible (Thermo Evolution Array) at 553 nm (Supplementary Material, Figure S5 and Figure S6). In order to verify the stability of the catalysts, five tests of reuse of the mesoporous graphitic carbon nitride with Tween-40 and mesoporous graphitic carbon nitride with Pluronic F127 were carried out for the degradation of rhodamine B, under the same conditions previously described (Supplementary Material, Figure S8).

### *Allium Cepa* bioassay

Bioassays with *Allium Cepa* were carried out to verify the effects of using the new catalyst on flora, and the methodology was based on the method proposed by Pittol et al. (2017) described below. The experiment consisted of initially solubilizing the mesoporous graphitic carbon nitride catalyst with Tween-40 in deionized water, and the suspension was maintained in an ultrasonic bath for 30 min. After this process, it was placed in a transparent flask and the sample of *Allium Cepa*, previously cleaned with deionized water was added. The solution resulting from the photocatalytic degradation test of rhodamine B catalyzed by mesoporous graphitic carbon nitride with Tween-40 was also used in the *Allium Cepa* bioassay, using the same method described above. The samples of deionized water and rhodamine B were called negative and positive controls. The tests were carried out for a period of 14 consecutive days at room temperature (Supplementary Material, Figure S9).

## Results and discussion

### Characterization of photocatalysts

Thermogravimetric and differential thermogravimetric analysis, Fig. 1a, b, were essential for understanding the synthesis of mesoporous graphitic carbon nitride, allowing a follow-up of the steps described in the mechanism of synthesis proposed by Yan et al. (2009), in which bulk graphitic carbon nitride was obtained from melamine pyrolysis.

In Fig. 1a, the pure melamine thermogravimetric curve (pink line) shows one mass loss event in 200–366 °C, corresponding to melamine sublimation, corresponding to approximately 100% mass loss. In this temperature range, melamine sublimation occurs, as described in the work of Yan et al. (2009) with no thermal condensation because the crucible was kept fully open during thermogravimetric analysis.

In the thermogravimetric and differential thermogravimetric curves of Tween-40 and Pluronic F127 (Fig. 1a, b), a simplified mass loss event can be observed, indicating the occurrence of two successive reactions that can be attributed to the thermal degradation profile of the surfactant, from 159 to 425 °C for Pluronic F127 (violet line) and for the Tween-40 of 150–460 °C (green line).

For the polymeric precursor with Pluronic F127 (Fig. 1c) if a mass loss is observed in the temperature range between 60 and 165 °C, this event can be attributed to the precursor polymer constitution water loss because the thermogravimetric profile of this step does not match the adsorption water outlet. The formation of the precursor polymer with water in its constitution was not observed when the Tween-40 surfactant was used, thus proving the specificity of the Pluronic F127 surfactant. Moreover, concerning the polymeric precursor with Pluronic F127 (marine blue line) and polymeric precursor with Tween-40 (orange line), three main mass loss events are observed.

The first event (I), over the range from 280 to 390 °C, as highlighted in the graph of the differential thermogravimetric curve (Fig. 1d), may be associated with melamine sublimation, which did not react in the formation of the precursor polymer because the beginning of the event is very close to the onset of the single melamine mass loss event.

The second event (II), over the range from 390 to 520 °C, suggests two successive reactions, as highlighted in the graph of the differential thermogravimetric curve (Fig. 1d); the first reaction is possibly related to the ammonia output, and the second reaction is possibly related to surfactant elimination. The degradation or exit temperatures of pure surfactants occurred at lower temperatures.

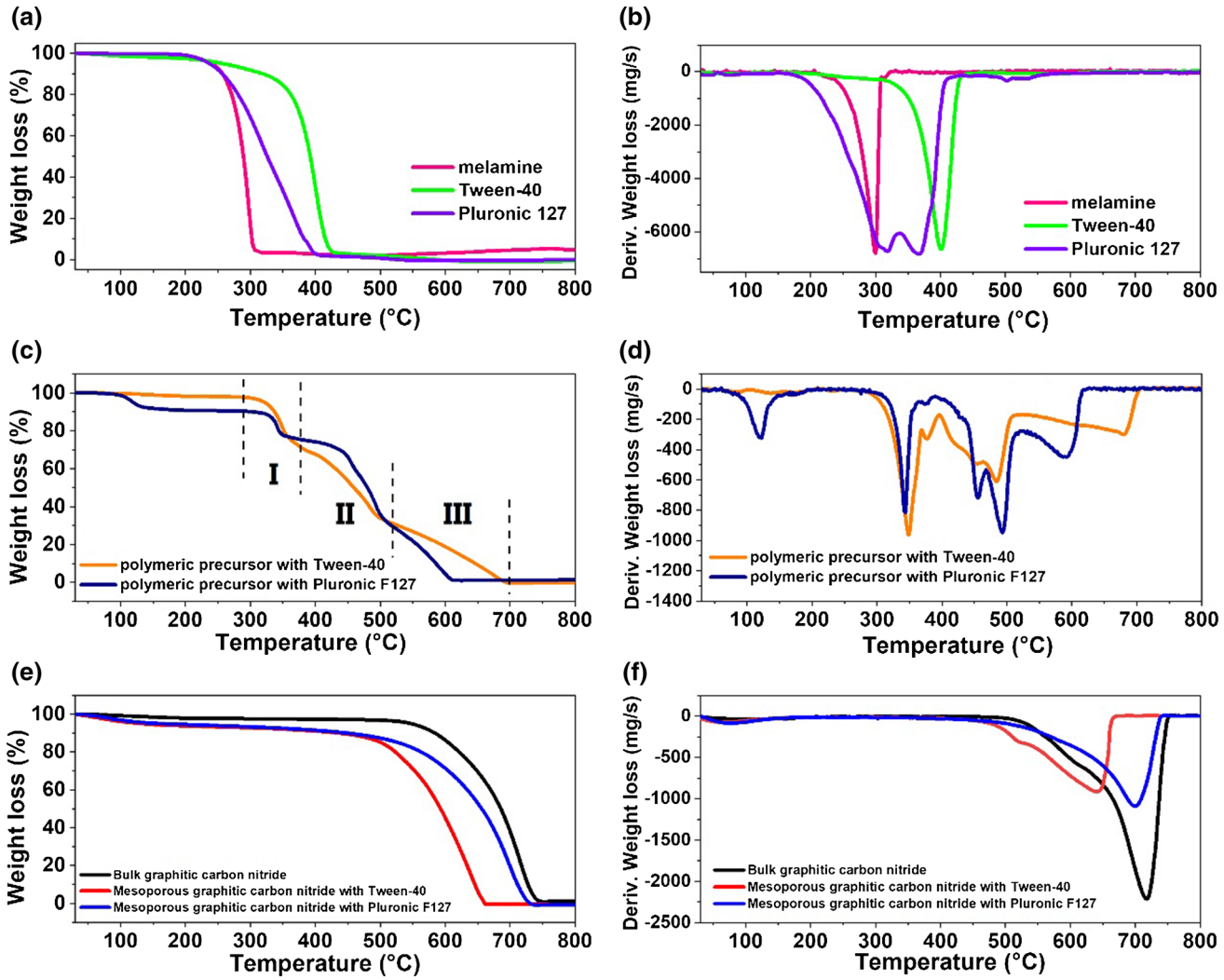


**Fig. 1** Thermogravimetric and differential thermogravimetric curves of the samples: pure melamine, Pluronic F127 and Tween-40 (**a**, **b**); polymeric precursor with Tween-40 and polymeric precursor with Pluronic F127 (**c**, **d**); mesoporous graphitic carbon nitride with Tween-40, mesoporous graphitic carbon nitride with Pluronic F127 and bulk graphitic carbon nitride (**e**, **f**). The thermogravimetric and differential thermogravimetric analyses describe the steps of the synthesis mechanism of bulk graphitic carbon nitride and mesoporous graphitic carbon nitride using Tween-40 and Pluronic F127 (see also Figure S4)

This phenomenon can be explained by the fact that the bonds between melamine and surfactant that are formed in the polymeric precursor give rise to graphitic carbon nitrides.

The third event (III), over the range from 520 to 630 °C, can be associated with the degradation of formed graphitic carbon nitride. According to Yan et al. (2009), the presence of endothermic peaks and the higher percentage of mass loss characterize the processes of deamination and thermal degradation of the material.

From the analysis of the thermogravimetric and differential thermogravimetric curves of the samples mesoporous graphitic carbon nitride with Tween-40, mesoporous graphitic carbon nitride with Pluronic F127 and bulk graphitic carbon nitride, as seen in Fig. 1e, f, we can observe similar decomposition profiles with two mass loss events.

The thermogravimetric curve of the bulk graphitic carbon nitride (black line) showed two events, the first from 69 to 191 °C, corresponding to approximately 2.5% of mass loss. Thermogravimetric curve of mesoporous graphitic carbon nitride with Tween-40 (red line) reveals the first event in the temperature range from 30 to 124 °C, which corresponds to 6.5% of mass loss. For sample mesoporous graphitic carbon nitride with Pluronic F127 (blue line), the first mass loss is observed in the temperature range of 46 to 120 °C, corresponding to approximately 6.3% of the mass loss, which can be attributed to water loss from surface adsorption (Yan et al. 2009; Hao et al. 2016). It is then observed that there is a greater predisposition of nitrides synthesized by the soft

template method to adsorb water molecules, probably due to the larger surface area.

As can be seen in Fig. 1e, f, the thermogravimetric and differential thermogravimetric curves reveal that the main mass loss event occurs at 714 °C for bulk graphitic carbon nitride, at 699 °C for graphitic carbon nitride mesoporous with Pluronic F127 and 644 °C for graphitic carbon nitride mesoporous with Tween-40, corresponding to approximately 96.5, 93.7 and 93.5% of mass loss, respectively.

In the temperature range 550–700 °C oxidation of graphitic carbon nitride occurs to form graphite and nitrogen ($N_2$) and at 740 °C oxidation of graphite in carbon dioxide ($CO_2$) (Li et al. 2008). Furthermore, mesoporous graphitic carbon nitride with Tween-40 and mesoporous graphitic carbon nitride with Pluronic F127 had lower thermal stability than the bulk graphitic carbon nitride, demonstrating that it is energetically and structurally more stable, as confirmed by X-ray diffraction results.

As seen in Fig. 2a, the X-ray diffraction pattern of bulk graphitic carbon nitride shows two characteristic peaks located at around 13.0° (100) and 27.4° (002) referring to the interlayer stacking of aromatic systems and the melon structural packaging formed by triple-unit units tri-s-triazines, respectively (Yan 2012).

The structure of mesoporous graphitic carbon nitride with Tween-40 and mesoporous graphitic carbon nitride with Pluronic F127 shows similarity to bulk graphitic carbon nitride, except for a subtle peak widening (002) and a notable decrease in peak intensity of 27.4°. Result similar to that was observed by Goettmann et al. (2006), relating it to the effect of geometric confinement on the walls of nanosized pores. In addition, there was a slight change in peak position 27.4° in the bulk graphitic carbon nitride to 27.21° in mesoporous graphitic carbon nitride with Tween-40 and 27.05° in mesoporous graphitic carbon nitride with Pluronic F127. Wu et al. (2019) relate the shift to a smaller angle to the increasing interlayer distance and associate decrease in peak intensity with defects in abundance.

Photoluminescence spectra, Fig. 2b, showed peaks in 444, 475, 508 and 535 nm, attributed to the π–π* transitions and n–π* emission (Wang et al. 2017) and also demonstrated a low-intensity peak located at 600 nm, which may originate from the nitrogen vacancy neutral charge state (Chidhambaram and Ravichandran, 2017).

Photoluminescence spectra showed the hypsochromic displacement of the emission bands of the mesoporous graphitic carbon nitride with Tween-40 and mesoporous graphitic carbon nitride with Pluronic F127, which is assigned to a band in the blue–violet region that indicated the existence of the π state in both samples (Zhang et al. 2013b), was observed gradual shift toward the blue region of the electromagnetic spectrum.

To understand the recombination dynamics of the photogenerated loads time-resolved fluorescence emission spectrometry was used. Two lifetimes were observed at four emission wavelengths, suggesting the existence of two species: one with a shorter life span, 0.20–0.68 ns, and another with a longer life span, between 2.09 and 3.31 ns. There was a decrease in the lifetime of mesoporous graphitic carbon nitride with Tween-40 and mesoporous graphitic carbon nitride with Pluronic F127 in relation to the bulk graphitic carbon nitride. However, the mesoporous graphitic carbon

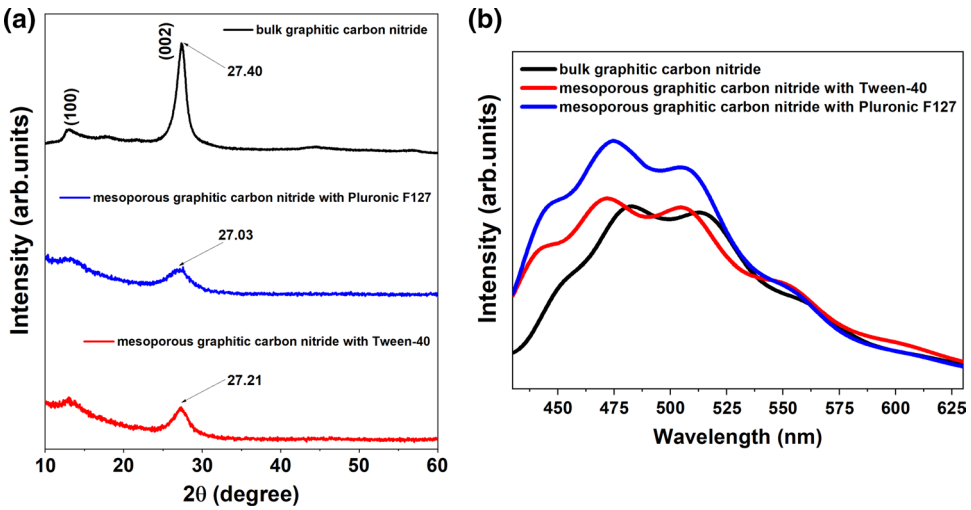


**Fig. 2** X-ray diffraction patterns of mesoporous graphitic carbon nitride with Tween-40, mesoporous graphitic carbon nitride with Pluronic F127 and bulk graphitic carbon nitride (**a**). The diffraction peaks decrease peak intensity (002) and, in addition, occurs the shift to a smaller angle, indicating the increase in defects and of the distance between layers. Photoluminescence spectra of mesoporous graphitic carbon nitride with Tween-40, mesoporous graphitic carbon nitride with Pluronic F127 and bulk graphitic carbon nitride (**b**). Comparing the samples, a gradual displacement toward the blue region of the electromagnetic spectrum was observed

nitride with Tween-40 showed a longer lifetime than the mesoporous graphitic carbon nitride with Pluronic F127. The decreasing electron lifetime indicates the existence of an additional channel for conduction band electron transfer to electronically trapped states may also be associated with the increase in defect density; the photogenerated electrons in the sample are captured by the defects at short distances (Ruan et al. 2018). Furthermore, according to Tian et al. (2017), the decrease in lifetime indicates that the photogenerated carriers of the sample are captured more quickly by reactive substrates and therefore are able to conduct redox reactions and also more efficient separation of electrons and holes.

The ultraviolet–visible reflectance spectra of mesoporous graphitic carbon nitride with Tween-40 and mesoporous graphitic carbon nitride with Pluronic F127, demonstrate that the use of surfactant causes the band gap variation between 2.77 and 2.84 eV for mesoporous graphitic carbon nitride with Tween-40 and mesoporous graphitic carbon nitride with Pluronic F127, respectively, suggesting a slight deviation of the blue absorption region of 0.28 and 0.20 eV from bulk graphitic carbon nitride (2.59 eV), associated with nitrogen vacancies and the effect of quantum confinement, in which photon-generated electron–hole pairs in the ultra-thin sheets can be quickly transferred along the surface, moving loads to reactive locations along the plane (Niu et al. 2012).

Nitrogen adsorption–desorption analysis was used to measure the Brunauer–Emmett–Teller surface area. As shown in Fig. 3a the isotherms indicated that the samples of mesoporous graphitic carbon nitride with Tween-40 and mesoporous graphitic carbon nitride with Pluronic F127 have Type IV behavior, meaning the formation of the mesoporous structure (Yan 2012; Tan et al. 2017).

Mesoporous graphitic carbon nitride with Tween-40 and mesoporous graphitic carbon nitride with Pluronic F127 obtained an increase in surface area of 28.2 and 27.9 $m^2\ g^{-1}$, respectively, compared to bulk graphitic carbon nitride with 8.8 $m^2\ g^{-1}$. Furthermore, as illustrated in Barrett–Joyner–Halenda (BJH) curve of Fig. 3b, there was an increased average pore diameter of mesoporous graphitic

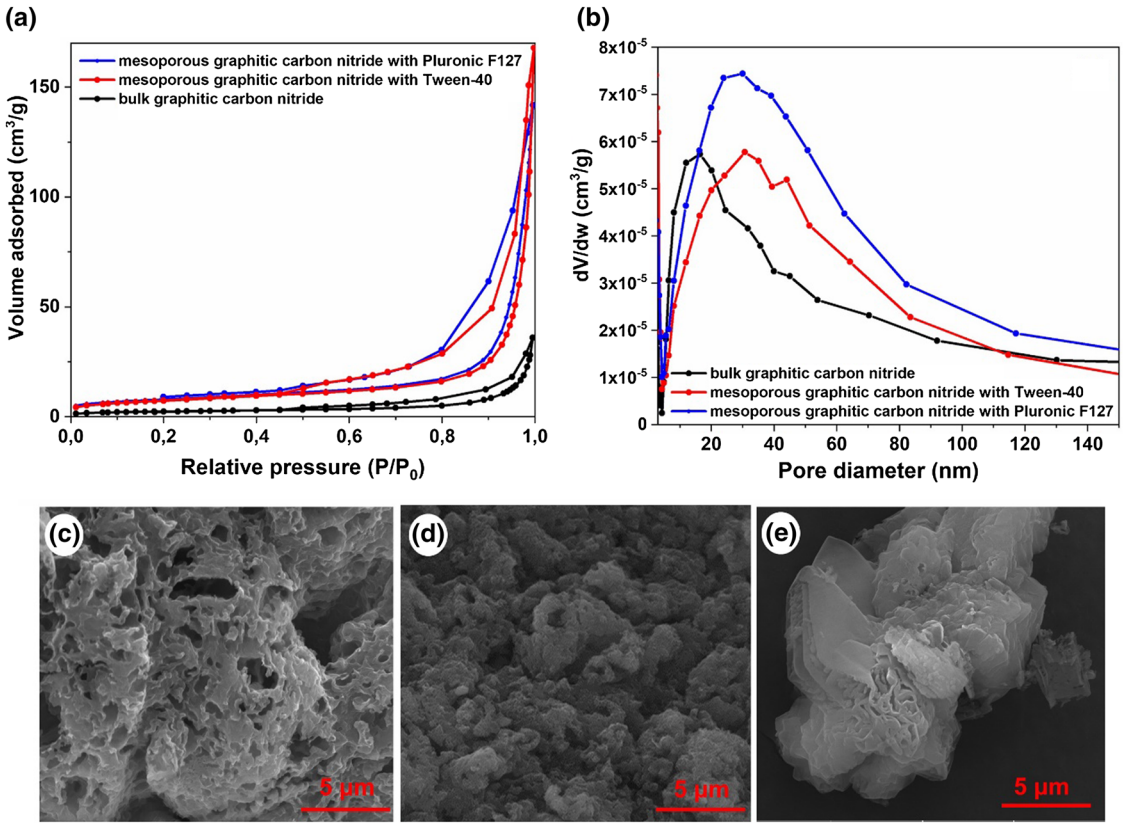


**Fig. 3** Nitrogen adsorption–desorption isotherm curves of samples (**a**). Pore size distribution curves of samples (**b**). Scanning electron microscopy image of samples: mesoporous graphitic carbon nitride with Tween-40 (**c**), mesoporous graphitic carbon nitride with Pluronic F127 (**d**) and bulk graphitic carbon nitride (**e**). Results indicated that mesoporous graphitic carbon nitride with Tween-40 and mesoporous graphitic carbon nitride with Pluronic F127 present typical mesoporous behavior. Besides, the use of surfactant increased the disorganization of the surface and the presence of small holes, mainly in the mesoporous graphitic carbon nitride with Tween-40 (see Table S1, Supplementary Material)

carbon nitride with Tween-40 and mesoporous graphitic carbon nitride with Pluronic F127, inducing the increase in light capture capacity and multiple dispersion effects by improving photocatalytic activity (Yan et al. 2010).

Figure 3 shows scanning electron microscope images of mesoporous graphitic carbon nitride with Tween-40 (Fig. 3c), mesoporous graphitic carbon nitride with Pluronic F127 (Fig. 3d) and bulk graphitic carbon nitride (Fig. 3e) with irregular surface formation of extremely thin leaf-like structures. In addition, the use of surfactant increased surface disorganization and the presence of small vacancies in all material, especially in the mesoporous graphitic carbon nitride with Tween-40. As corroborated by transmission electron microscopy image of the mesoporous graphitic carbon nitride with Tween-40, the typical structure of mesoporous materials (Jiang et al. 2017) with a nanoporous network are with pores approximately 10–50 nm.

## Mechanism of formation of mesoporous graphitic carbon nitride

Tween-40 is a nonionic surfactant that has a very special shape that favors the formation of mesopores. The mechanism of formation of mesoporous structures from the use of the surfactant Tween-40 has already been well reported in the literature for other materials in the researches carried out by Suh and Rhee (2003) and García-Benjume et al. (2009).

In this work, for the formation of mesoporous graphitic carbon nitride, initially, the neutral amines of precursor (melamine) and the nonionic surfactant Tween-40 are initially partially protonated or charged with the addition of the acid solution ($H_2SO_4$), causing electrostatic interactions and hydrogen bonds between the melamine and the surfactant (Yang et al. 1998; Ha and Park 2018); during the aging process, the formation of the polymeric precursor of mesoporous graphitic carbon nitride occurs. The mesoporous structure of graphitic carbon nitride is finally obtained after the calcination process of the polymeric precursor, as corroborated by the thermogravimetric analysis results, and the polymerization of polymeric precursor with Tween-40 in mesoporous graphitic carbon nitride with Tween-40 occurs simultaneously with the elimination of surfactant. Subsequent structural, textural and morphological analyses confirm that the structural organization was maintained and there is evidence of formation of mesoporous material.

## Photocatalytic performance and degradation mechanism of rhodamine B

Figure 4a shows the relative degradation ($C/C_0$) in relation to the irradiation time. ($C_0$ is the concentration of rhodamine B (mg $L^{-1}$) in the adsorption equilibrium before irradiation, and $C$ is the concentration of rhodamine B (mg $L^{-1}$) at the time ($t$) of reaction.) Mesoporous graphitic carbon nitride with Tween-40 showed higher photodegradation of rhodamine B compared to bulk graphitic carbon nitride and graphitic carbon nitride with Pluronic F127, eliminating 93.0% of rhodamine B after 60 min of visible-light irradiation, where the bulk graphitic carbon nitride degraded only 30.5% and graphitic carbon nitride with Pluronic F127 degraded 86.0%.

After 120 min of reaction the bulk graphitic carbon nitride degraded 58.8% of rhodamine B, while the samples of mesoporous graphitic carbon with Tween-40 and mesoporous graphitic carbon nitride with Pluronic F127 achieved 100% rhodamine B degradation, but in mesoporous graphitic carbon nitride with Tween-40 degradation was faster throughout the process. The high catalytic performance observed for mesoporous graphitic carbon nitride with Tween-40 was associated with a larger surface area (28.2 $m^2$ $g^{-1}$), a larger pore diameter and volume (29.5 and 0.234 nm), mesoporous morphology, in addition to the increase in the defect density of nitrogen vacancies, which were confirmed using textural and optical analysis by photoluminescence spectroscopy, nitrogen adsorption–desorption analysis and by scanning and transmission electron microscopy images.

As seen in Fig. 4b, the graph of the degradation kinetics of rhodamine B for the evaluated samples suggests that the degradations of the present study follow a pseudofirst-order kinetic model, and results similar to those reported by Wang et al. (2016) and photo-degradation of rhodamine B were carried out in the research conducted by Saeed et al. (2018).

The absorption spectra of rhodamine B exhibited a significant reduction in the vibrational mode at 553 nm, characteristic of chromophore groups of rhodamine B (He et al. 2009). Thus, it can be clarified that the mesoporous graphitic carbon nitride with Tween-40 and mesoporous graphitic carbon nitride with Pluronic F127 photocatalysts are highly effective for the degradation of rhodamine B under visible light.

During the photocatalytic process some active species can be formed, such as hydroxyl, superoxides and holes radicals. In general, the hydroxyl radical stems from direct hole oxidation or electron-induced dynamic reduction; in turn, superoxide formation is associated with direct photogenerated electron-induced oxygen reduction (Yan et al. 2009). To investigate the possible photocatalytic mechanism of rhodamine B degradation through mesoporous graphitic carbon nitride with Tween-40 and mesoporous graphitic carbon nitride with Pluronic F127 catalysts, experiments were performed with the addition of hydroxyl, superoxide and hole radical markers, such as isopropyl alcohol, benzoquinone and ammonium oxalate. Based on the results obtained

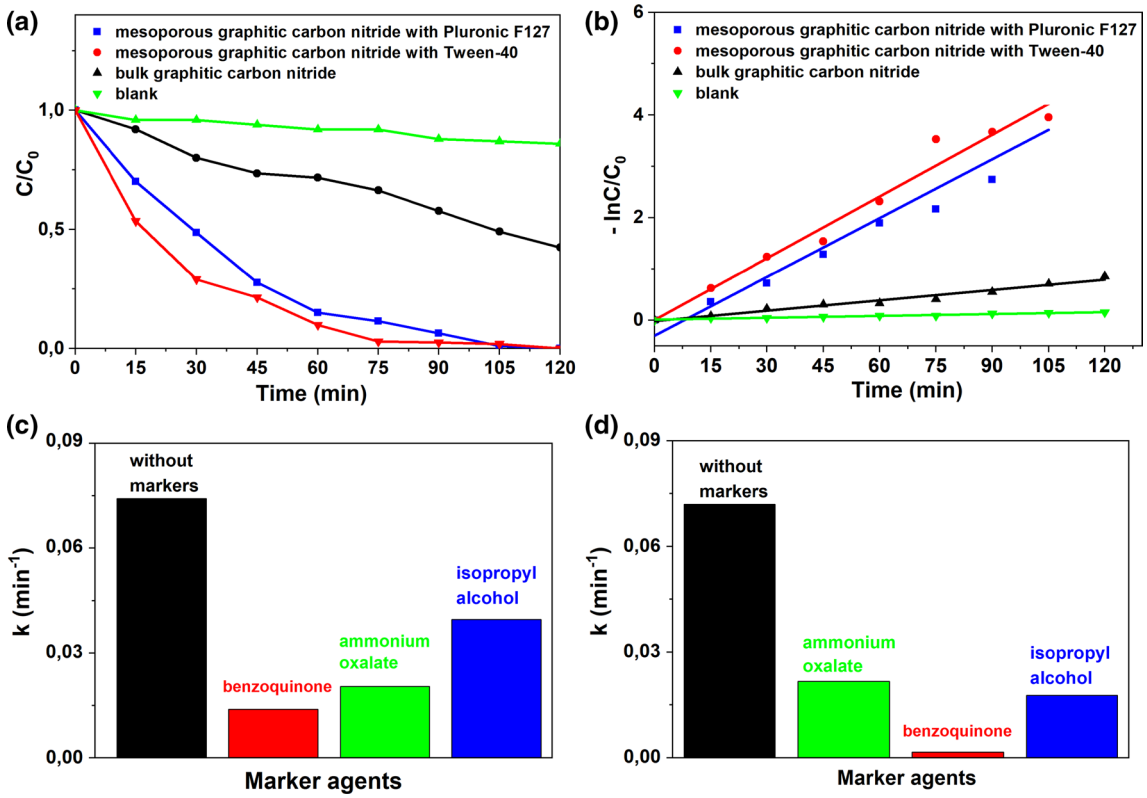


**Fig. 4** Relative photodegradation $C/C_0$ ($C$ is the concentration of rhodamine B (mg $L^{-1}$), $C_0$ is the concentration of rhodamine B in the adsorption equilibrium before irradiation) against time (min) (**a**). Pseudofirst-order kinetic fitting (**b**). Reaction rate constant ($k$) in the presence of markers agents using mesoporous graphitic carbon nitride with Pluronic F127 (**c**) and mesoporous graphitic carbon nitride with Tween-40 (**d**). In the blank test (without catalyst), rhodamine B was very stable during lighting, but the mesoporous graphitic carbon nitride with Tween-40 and Pluronic F127 showed superior degradation in comparison with the bulk graphitic carbon nitride. Moreover, on presence of benzoquinone, there was a decrease in the rate of degradation, suggesting that superoxide radicals are the main active species (see also Figure S6 and Figure S7)

by ultraviolet–visible reflectance absorption spectra, the degradation rate of the organic pollutant was calculated.

As can be seen in Fig. 4c, d, the photocatalytic performance of rhodamine B with the addition of isopropyl alcohol did not significantly inhibit the catalytic action of mesoporous graphitic carbon nitride with Pluronic F127 and mesoporous graphitic carbon nitride with Tween-40, implying that hydroxyl played a role relatively minor in the photocatalytic reaction. The addition of ammonium oxalate had a weak influence with subtle inhibition of the catalyst. However, in the presence of benzoquinone, there was a considerable decrease in the rate of rhodamine B degradation, suggesting that superoxide radicals are the main species active in the degradation of rhodamine B by mesoporous graphitic carbon nitride with Tween-40 and mesoporous graphitic carbon nitride with Pluronic F127.

Similar results were found in studies carried out by Hao et al. (2016), in which the photocatalytic performance of rhodamine B degradation catalyzed by mesoporous graphitic carbon nitride decreased dramatically after the addition of superoxide and hole inhibitors, suggesting that these radicals were the main species reactive. In the work carried out by Iqbal et al. (2017), superoxide radicals and holes were also essential for the photodegradation of rhodamine B under visible light.

In the recent research conducted by Xia et al. (2019) evaluated the yield of photoelectrons by detecting superoxide radicals in photocatalytic reactions based on graphitic carbon nitride obtained from melamine and urea, the results of electron paramagnetic resonance spectroscopy (EPR) revealed that both graphitic carbon nitrides synthesized can thermodynamically produce superoxide radicals under lighting, as the conduction band (CB) positions are more negative than the potential for $O_2/O_2^-$ (−0.33 V, NHE: normal hydrogen electrode). It was found that both graphitic carbon nitride samples produce $O_2$; however, they do not produce hydroxyl radicals under lighting, due to the graphitic carbon nitride obtained from melamine and urea valence band (VB) positions more positive than the $H_2O/O_2$ potential (0.82 V, NHE: normal hydrogen electrode), but less positive than

the $H_2O/^{\cdot}OH$ potential (2.34 V, NHE: normal hydrogen electrode).

To evaluate the stability five mesoporous graphitic carbon nitride with Tween-40 and mesoporous graphitic carbon nitride with Pluronic F127 catalyst reuse tests. After five cycles of use, the catalysts showed 100% rhodamine B degradation, thus demonstrating its excellent recyclability.

### *Allium Cepa* bioassays

*Allium Cepa* bioassays can evaluate the genotoxic potential of textile dye-contaminated effluents such as rhodamine B. Genotoxicity is associated with the presence of azo dyes and aromatic amines present in dyes of the industrial effluent tested (Sudhakar et al. 2001; Pittol et al. 2017).

The photographs show the root growth of the *Allium Cepa* species when compared to the sample containing negative control (deionized water); it was observed that the tests containing the mesoporous graphitic carbon nitride catalyst did not present damage to the structures of the onion samples. In contrast, the rhodamine B solution test (positive control) showed a reduced development of the *Allium Cepa* root. According to Pittol et al. (2017), this root reduction may be related to changes in the division cycle and damage to DNA. Thus, it is suggested that the use of mesoporous graphitic carbon nitride with Tween-40 catalysts for photocatalytic degradation of rhodamine B does not cause damage to the flora.

## Conclusion

The photocatalysts mesoporous graphitic carbon nitride was prepared via the soft template method for the first time using Tween-40 as a template for mesoporous graphitic carbon nitrides. For comparison purposes, catalysts were also synthesized using the Pluronic F127 surfactant as a template, in addition to bulk graphitic carbon nitride. Structural analysis revealed that the mesoporous graphitic carbon nitride polymeric structure was maintained; however, electronic properties were altered, causing not only light absorption with slight deviation from the blue absorption region but also improved electronic conductivity. The textural characteristics were significantly altered, resulting in a high surface area, larger diameter and pore volume. The morphological analyses showed a mesoporous and nanopore construction that guaranteed the largest number of sites available for the photocatalytic reaction, contributing to the excellent photocatalytic degradation performance of pollutants under visible-light irradiation. Bioassays with *Allium Cepa* species revealed that the samples synthesized by this method do not cause damage to the environment. Therefore, the mesoporous graphitic carbon nitride possesses great potential for application in water treatment.

**Acknowledgements** The authors gratefully acknowledge the Federal University of Pará, Laboratory of the Research and Analysis of Fuels, Laboratory of Amazon Oils, Laboratory of Catalysis Oilchemistry and Laboratory of Spectroscopy network for the support of the parties facilitated in this work and Pro-rectory of research and post-graduation. This study was financed in part by the Coordenação de Aperfeiçoamento de Pessoal de Nível Superior—Brasil (CAPES)—Finance Code 001.

## References

Boissiére C et al (2000) A new synthesis of mesoporous MSU-X silica controlled by a two-step pathway. Chem Mater 12:2902–2913. https://doi.org/10.1021/cm991188s

Chen Y et al (2011) Synthesis, characterization and electrochemical properties of mesoporous zirconia nanomaterials prepared by self-assembling sol–gel method with Tween 20 as a template. Chem Eng J 170:518–524. https://doi.org/10.1016/j.cej.2010.09.063

Chen X et al (2016) Growth of g-$C_3N_4$ on mesoporous $TiO_2$ spheres with high photocatalytic activity under visible light irradiation. Appl Catal B Environ 188:342–350. https://doi.org/10.1016/j.apcatb.2016.02.012

Chidhambaram N, Ravichandran K (2017) Single step transformation of urea into metal-free g-$C_3N_4$ nanoflakes for visible light photocatalytic applications. Mater Lett 207:44–48. https://doi.org/10.1016/j.matlet.2017.07.040

Fang S et al (2015) Effect of acid on the photocatalytic degradation of rhodamine B over g-$C_3N_4$. Appl Surf Sci 358:336–342. https://doi.org/10.1016/j.apsusc.2015.07.179

García-Benjume ML, Espitia-Cabrera MI, Contreras-García ME (2009) Hierarchical macro-mesoporous structures in the system $TiO_2$–$Al_2O_3$, obtained by hydrothermal synthesis using Tween-20® as a directing agent. Mater Charact 60:1482–1488. https://doi.org/10.1016/j.matchar.2009.08.003

Goettmann F et al (2006) Chemical synthesis of mesoporous carbon nitrides using hard templates and their use as a metal-free catalyst for Friedel–Crafts reaction of benzene. Angew Chem Int Ed 45:4467–4471. https://doi.org/10.1002/anie.200600412

Gong W et al (2015) Nickel oxide and nickel co-doped graphitic carbon nitride nanocomposites and its octylphenol sensing application. Electroanalysis 28:227–234. https://doi.org/10.1002/elan.201500491

Ha C-S, Park SS (2018) General synthesis and physico-chemical properties of mesoporous materials. Springer, Berlin, pp 15–85. https://doi.org/10.1007/978-981-13-2959-3_2

Hao R et al (2016) Template-free preparation of macro/mesoporous g-$C_3N_4$/$TiO_2$ heterojunction photocatalysts with enhanced visible light photocatalytic activity. Appl Catal B Environ 187:47–58. https://doi.org/10.1016/j.apcatb.2016.01.026

He Z et al (2009) Photocatalytic degradation of rhodamine B by $Bi_2WO_6$ with electron accepting agent under microwave irradiation: Mechanism and pathway. J Hazard Mater 162:1477–1486. https://doi.org/10.1016/j.jhazmat.2008.06.047

Iqbal W et al (2017) Eco-friendly one-pot synthesis of well-adorned mesoporous g-$C_3N_4$ with efficiently enhanced visible light photocatalytic activity. Catal Sci Technol 7:1726–1734. https://doi.org/10.1039/C7CY00286F

Jiang X et al (2017) The photocatalytic performance of g-$C_3N_4$ from melamine hydrochloride for dyes degradation with

peroxymonosulfate. J Photochem Photobiol A Chem 336:54–62. https://doi.org/10.1016/j.jphotochem.2016.12.018
Kishore RSK et al (2011) Degradation of polysorbates 20 and 80: studies on thermal autoxidation and hydrolysis. J Pharm Sci 100:721–731. https://doi.org/10.1002/jps.22290
Kumar A, Thakur PR, Sharma G et al (2019) Carbon nitride, metal nitrides, phosphides, chalcogenides, perovskites and carbides nanophotocatalysts for environmental applications. Environ Chem Lett 17:655–682. https://doi.org/10.1007/s10311-018-0814-8
Li X et al (2008) Preparation and characterization of graphitic carbon nitride through pyrolysis of melamine. Appl Phys A 94:387–392. https://doi.org/10.1007/s00339-008-4816-4
Li F et al (2014) Precipitation synthesis of mesoporous photoactive $Al_2O_3$ for constructing g-$C_3N_4$-based heterojunctions with enhanced photocatalytic activity. Ind Eng Chem Res 53:19540–19549. https://doi.org/10.1021/ie5036258
Liang C et al (2008) Mesoporous carbon materials: synthesis and modification. Angew Chem Int Ed 47:3696–3717. https://doi.org/10.1002/anie.200702046
Ma R et al (2017) Eco-friendly photocatalysts achieved by zeolite fixing. Appl Catal B Environ 212:193–200. https://doi.org/10.1016/j.apcatb.2017.04.071
Niu P et al (2012) Nitrogen vacancy-promoted photocatalytic activity of graphitic carbon nitride. J Phys Chem C 116:11013–11018. https://doi.org/10.1021/jp301026y
Osman H, Su Z, Ma X (2017) Efficient photocatalytic degradation of Rhodamine B dye using ZnO/graphitic $C_3N_4$ nanocomposites synthesized by microwave. Environ Chem Lett 15:435–441. https://doi.org/10.1007/s10311-017-0604-8
Peer M et al (2017) Facile soft-templated synthesis of high-surface area and highly porous carbon nitrides. Chem Mater 29:1496–1506. https://doi.org/10.1021/acs.chemmater.6b03570
Pittol M et al (2017) Macroscopic effects of silver nanoparticles and titanium dioxide on edible plant growth. Environ Nanotechnol Monit Manag 8:127–133. https://doi.org/10.1016/j.enmm.2017.07.003
Poła M, Ćirin D (2012) Mixed micelles of sodium salts of bile acids and Tween 40: effect of the steroid skeleton on the coefficient of interaction in mixed micelles. Ind Eng Chem Res 51:14722–14728. https://doi.org/10.1021/ie301648h
Ruan D et al (2018) Defects rich g-$C_3N_4$ with mesoporous structure for efficient photocatalytic $H_2$ production under visible light irradiation. Appl Catal B Environ 238:638–646. https://doi.org/10.1016/j.apcatb.2018.07.028
Saeed M, Ahmad A, Boddula R et al (2018) Ag@MnxOy: an effective catalyst for photo-degradation of rhodamine B dye. Environ Chem Lett 16:287–294. https://doi.org/10.1007/s10311-017-0661-z
Sudhakar R et al (2001) Mitotic abnormalities induced by silk dyeing industry effluents in the cells of *Allium Cepa*. Cytologia 66:235–239. https://doi.org/10.1508/cytologia.66.235
Suh Y, Rhee H (2003) Synthesis of stable mesostructured zirconia: Tween surfactant and controlled template removal. Korean J Chem Eng 20:65–70. https://doi.org/10.1007/bf02697186
Tan S et al (2017) Meso-g-$C_3N_4$/g-$C_3N_4$ nanosheets laminated homojunctions as efficient visible-light-driven photocatalysts. Int J Hydrogen Energy 42:25969–25979. https://doi.org/10.1016/j.ijhydene.2017.08.202
Tian N et al (2017) Precursor-reforming protocol to 3D mesoporous g-$C_3N_4$ established by ultrathin self-doped nanosheets for superior hydrogen evolution. Nano Energy 38:72–81. https://doi.org/10.1016/j.nanoen.2017.05.038
Tonda S et al (2014) Fe-doped and -mediated graphitic carbon nitride nanosheets for enhanced photocatalytic performance under natural sunlight. J Mater Chem A 2:6772–6780. https://doi.org/10.1039/c3ta15358d
Wang Y et al (2010) Facile one-pot synthesis of nanoporous carbon nitride solids by using soft templates. Chemsuschem 3:435–439. https://doi.org/10.1002/cssc.200900284
Wang Y et al (2011) Polymeric graphitic carbon nitride as a heterogeneous organocatalyst: from photochemistry to multipurpose catalysis to sustainable chemistry. Angew Chem Int Ed 51:68–89. https://doi.org/10.1002/anie.201101182
Wang P et al (2016) Efficient degradation of organic pollutants and hydrogen evolution by g-$C_3N_4$ using melamine as the precursor and urea as the modifier. RSC Adv 6:33589–33598. https://doi.org/10.1039/c5ra26890g
Wang Y et al (2017) Linker-controlled polymeric photocatalyst for highly efficient hydrogen evolution from water. Energy Environ Sci 10:1643–1651. https://doi.org/10.1039/c7ee01109a
Wu M et al (2019) Template-free synthesis of nanocage-like g-$C_3N_4$ with high surface area and nitrogen defects for enhanced photocatalytic $H_2$ activity. J Mater Chem 7:5324–5332. https://doi.org/10.1039/C8TA12076E
Xia P et al (2019) Localized π-conjugated structure and EPR investigation of g-$C_3N_4$ photocatalyst. Appl Surf Sci 487:335–342. https://doi.org/10.1016/j.apsusc.2019.05.064
Xiong W et al (2012) Preparation of nitrogen-doped macro-/mesoporous carbon foams as electrode material for supercapacitors. Colloids Surf A Physicochem Eng Asp 411:34–39. https://doi.org/10.1016/j.colsurfa.2012.06.042
Yan H (2012) Soft-templating synthesis of mesoporous graphitic carbon nitride with enhanced photocatalytic $H_2$ evolution under visible light. Chem Commun 48:3430–3432. https://doi.org/10.1039/c2cc00001f
Yan SC et al (2009) Photodegradation performance of g-$C_3N_4$ fabricated by directly heating melamine. Langmuir 25:10397–10401. https://doi.org/10.1021/la900923z
Yan SC, Li ZS, Zou ZG (2010) Photodegradation of Rhodamine B and methyl orange over boron-doped g-$C_3N_4$ under visible light irradiation. Langmuir 26:3894–3901. https://doi.org/10.1021/la904023j
Yang P et al (1998) Generalized syntheses of large-pore mesoporous metal oxides with semicrystalline frameworks. Nature 396:152–155. https://doi.org/10.1038/24132
Zhang Z et al (2013a) Biopolymer-activated graphitic carbon nitride towards a sustainable photocathode material. Sci Rep 3:1–5. https://doi.org/10.1038/srep02163
Zhang Y et al (2013b) Synthesis and luminescence mechanism of multicolor-emitting g-$C_3N_4$ nanopowders by low temperature thermal condensation of melamine. Sci Rep 3:1–8. https://doi.org/10.1038/srep01943
Zhang X, Yuan L, Liang F et al (2019) Water-assisted synthesis of shape-specific BiOCl nanoflowers with enhanced adsorption and photosensitized degradation of rhodamine B. Environ Chem Lett 18:243–249. https://doi.org/10.1007/s10311-019-00929-2